JBC RESEARCH ARTICLE

The *Pseudomonas aeruginosa* PhuS proximal ligand His-209 triggers a conformational switch in function from DNA binding to heme transfer

Received for publication, November 16, 2024, and in revised form, February 22, 2025 Published, Papers in Press, March 22, 2025,
https://doi.org/10.1016/j.jbc.2025.108440

Nicholas Montes[1], Tyree Wilson[2], Samuel A. Krug[1], Susana Mouriño[1], Maureen A. Kane[1], Daniel Deredge[1], and Angela Wilks[1,*]

From the [1]Department of Pharmaceutical Sciences, School of Pharmacy, University of Maryland, Baltimore, Maryland, USA; [2]Molecular Pathogenesis and Biomarkers Section, National Institute of Allergy and Infectious Disease, Rockville, Maryland, USA

Reviewed by members of the JBC Editorial Board. Edited by Donita C. Brady

Pseudomonas aeruginosa **can acquire iron from heme *via* the heme assimilation system and *Pseudomonas* heme uptake (Phu) systems. Heme uptake is regulated at the metabolic level by the cytoplasmic protein PhuS that controls heme flux through a heme oxygenase HemO, releasing iron and biliverdin IXβ and IXδ. We have shown PhuS regulates extracellular heme flux, and in its apo-form transcriptionally regulates the iron and heme-dependent small RNAs (sRNAs) PrrF/PrrH. This mutual exclusivity of function is driven by conformational rearrangement of PhuS on heme binding. Herein, we show through a combination of EMSA and fluorescence anisotropy that mutation of the His-209 proximal ligand allows both apo- and holo-PhuS H209A to bind to the *prrF1* promoter with significantly lower affinity when compared to PAO1 WT. Hydrogen deuterium exchange coupled to mass spectrometry revealed the apo- and holo-PhuS H209A structures are closer to each other than their WT counterparts and sample a conformational landscape between the apo- and holo-PhuS WT conformations, that is neither optimal for heme transfer nor DNA-binding. Furthermore, quantitative PCR and Western blot analysis of the *phuSH209A* allelic strain compared to PAO1 WT revealed an uncoupling of the PhuS-HemO dependent regulation of heme flux into the cell that abrogates the heme dependent regulation of the PrrF/PrrH sRNAs. The data supports a model where heme coordination through His-209 drives the conformational switch that determines mutual exclusivity in function of apo- and holo-PhuS. This dual function of PhuS is central to integrating extracellular heme utilization into the PrrF/PrrH sRNA regulatory network critical for *P. aeruginosa* adaptation within the host.**

The gram-negative opportunistic pathogen *Pseudomonas aeruginosa* must acquire iron from the host for its survival and ability to establish infection. However, due to its reactivity, iron is tightly regulated and sequestered in iron-binding proteins such as transferrin and ferritin, or in heme and iron-sulfur cluster containing proteins. Iron is further limited within the host during infection by the activation of the innate immune response that includes the hepcidin dependent downregulation of plasma iron levels, and the secretion of high affinity iron binding proteins such as lipocalin 2 (1). To overcome this nutritional immunity *P. aeruginosa* possesses several acquisition strategies to obtain iron *via* siderophore secretion or the utilization of heme (2–5). *P. aeruginosa* encodes two heme uptake systems; the heme assimilation system (Has) and the *Pseudomonas* heme uptake (Phu) system (6). The Has and Phu systems were shown to have non-redundant roles in heme sensing and transport, respectively (7). The secreted hemophore HasAp on interaction with the OM receptor HasR triggers activation of the extra cytoplasmic function σ/anti-σ factor system HasIS. The HasI σ factor leads to transcriptional amplification of the *has* operon (8). However, heme transported by either the HasR or PhuR outer membrane receptors is translocated to the cytoplasm by the *phu* encoded ABC transporter PhuUV, and its cognate periplasmic protein PhuT. Previous studies from our laboratory have shown the cytoplasmic heme binding protein PhuS regulates the heme flux into the cell through its specific interaction with the iron regulated heme oxygenase, HemO (9, 10). HemO oxidatively cleaves heme to release iron, CO, and biliverdin (BV) IXβ and IXδ (11). Interestingly, the BVIXβ metabolite post transcriptionally regulates HasAp (8). Thus, the PhuS-HemO couple regulates both heme flux into the cell, and extracellular heme sensing *via* the heme metabolites. Furthermore, the recent evidence of the integration of extracellular heme metabolism *via* the BVIXβ metabolite with the transition from planktonic to sessile lifestyle further highlights the central role of extracellular heme metabolism in *P. aeruginosa* pathogenesis (12).

Previously, we have shown the cytoplasmic heme binding protein PhuS in addition to regulating heme flux through HemO, in its apo-form binds to the *prrF1* promoter of the tandem *prrF1, prrF2* small RNA locus (13). The PrrF small RNAs (sRNAs) are highly homologous to one another and contribute to iron homeostasis by promoting mRNA degradation of nonessential iron-containing proteins (14–16). The PrrF sRNAs also play a role in other cellular processes

* For correspondence: Angela Wilks, awilks@rx.umaryland.edu.

including twitching motility and biosynthesis of quorum sensing molecules (15, 17). Furthermore, this tandem arrangement allows for the expression of an overlapping noncoding RNA, PrrH, whose expression is heme-dependent (18). The tandem arrangement of the *prrF* genes and the presence of *phuS* are found only in pathogenic *P. aeruginosa* and not in other Pseudomonads, highlighting the significance of this genetic arrangement to virulence (18). Furthermore, PrrH is detected in infected murine lungs as well as sputum from cystic fibrosis patients suggesting a role for this heme-dependent sRNA during infection (19). Our previous *in vitro* studies showed apo-PhuS binds with high affinity to the promoter of *prrF1* but not that of *prrF2* (13). The *prrF1* and *prrF2* genes are independently regulated by the ferric uptake regulator (Fur) and as the *prrF1* apo-PhuS binding site overlaps with the Fur box, this allows for differential regulation of PrrF1 and PrrF2 at intracellular iron levels that would otherwise lead to Fur repression. Furthermore, comparison of the relative expression of PrrF and PrrH in the PAO1 WT and the Δ*phuS* allelic strain showed a loss in the heme dependent regulation of PrrH in the absence of PhuS (13). The mechanism by which the heme dependent read through of the *prrF1/F2* intergenic region yields PrrH is not known, but based on the present data and previous results it is dependent on the dual function of PhuS as a heme chaperone and transcriptional regulator (13). To further investigate the mechanism by which PhuS is able to partition its heme transfer and DNA binding functions, several variants were constructed targeting His residues located within the heme binding C-terminal domain including His-209, the heme proximal ligand and His-212 previously proposed to facilitate heme transfer to HemO (20, 21). Hydrogen deuterium exchange coupled to mass spectrometry (HDX-MS) studies on apo- and holo-PhuS revealed that in the apo-form the C-terminal α6/7/8 helices encompassing the heme coordinating residues are largely labile and unstructured, and following heme binding and subsequent coordination the protein undergoes a conformational rearrangement which results in rigidification and protection from deuterium exchange (21). The rearrangement from an open heme binding cleft to the closed conformation is required for the interaction with HemO. Additionally, holo-PhuS after initial structural rearrangement undergoes localized folding and unfolding within the C-terminal α6/7/8 helices that are coupled to similar rates of exchange in the N-terminal α1/2 helices. In contrast, the holo-PhuS H212R variant which is impaired in its ability to transfer heme to HemO is more structured, and the regions of allosteric cooperativity that map to the PhuS:HemO interface are significantly dampened. The more structured C terminus and decrease in conformational flexibility in the apo-PhuS H212R also reduced the DNA binding affinity ∼1.5-fold indicating that conformational reorganization and structural dynamics within this region is the major driver of function in PhuS. Herein, employing a combination of biophysical, biochemical, and genetic approaches we further investigated the role of heme coordination and protein dynamics in the PhuS H209A variant where heme coordination through His-212 represents an intermediate state in heme transfer and DNA binding. These studies will advance our understanding of heme and iron homeostasis and the contribution of PhuS to *P. aeruginosa* adaptation and survival within the host.

Results

Apo- and holo-PhuS H209A bind to the prrF1 promoter

Previous EMSA studies have shown apo- but not holo-PhuS binds to the *prrF1* promoter (13). Utilizing the identical *prrF1-50* 5′-biotinylated probe (Table S2) we confirmed the apo-H209A binds to the *prrF1-50* probe. Addition of increasing concentrations of apo-PhuS H209A to the *prrF1-50* 5′-biotinylated probe gave a lower mobility band (LMB) consistent with binding of the protein to the probe (Fig. 1*A*). The reconstituted holo-PhuS H209A similar to holo-PhuS WT had a heme occupancy of ≥95% as judged by pyridine hemochrome. Interestingly, the addition of increasing concentrations of holo-PhuS H209A showed a similar shift (Fig. 1*B*). However, we observed more than one LMB which is not apparent with either apo-H209A or apo-PhuS. To determine if holo-PhuS H209A on binding to the *prrF1* promoter retains

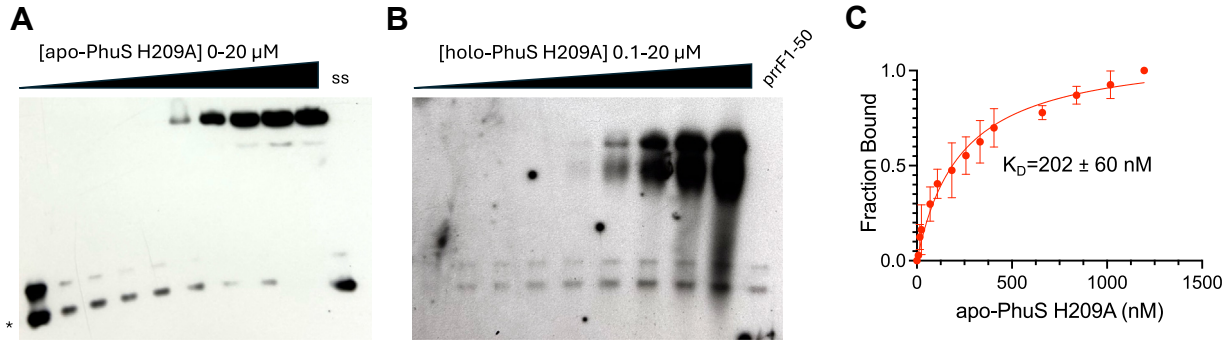

Figure 1. EMSA and FA of apo- and holo-PhuS H209A binding to *prrF1-50*. apo-PhuS H209A (*A*) and holo-PhuS H209A (*B*) binding to 5′-biotin-labeled *prrF1-50*. Apo-PhuS binding to 5′-FAM-labeled *prrF1-50* (*C*). Experiments were performed as described in Experimental procedures section. All EMSA reactions contained a fixed concentration (30 pM) of labeled *prrF1-50* or *prrF1-50s* (scrambled sequence) and following incubation were run on 8% acrylamide gels and transferred to a nylon membrane and visualized by chemiluminescence. Apo- or holo-PhuS concentrations were as follows (0.1, 0.2, 0.3,0.4, 0.5, 1.0, 5.0, 10, and 20 μM). The scrambled sequence was run in the presence of 20 μM apo-PhuS. FA experiments were performed in triplicate as described and the data were fit by converting the anisotropy, *r*, to fraction bound and plotted against protein concentration using a one-site binding model. The error is shown as SEM. *Denotes a second band due to degradation of the probe. FA, fluorescence anisotropy.

the heme or is displaced on DNA binding, we analyzed the protein–DNA complex by size-exclusion chromatography (SEC). Interestingly, the PhuS-DNA complex that eluted from the column does not retain the heme, indicating that DNA binding to holo-H209A effectively displaces the heme, with the remaining holo-PhuS complex eluting in a later fraction (Fig. S1). Previous resonance Raman studies confirmed heme is coordinated to His-212 in the absence of His-209, but with a four-fold reduction in the heme binding affinity ($K_D \sim 1.6$ μM *versus* ~ 0.4 μM for the PhuS WT) (20). Additionally, previous studies on the kinetics of heme binding in Phus WT, together with the binding affinity, had suggested that a slow heme off rate is a major contributor to kinetically trapping heme on His-209 (21). In contrast, heme coordinated through His-212 is effectively displaced by DNA suggesting an increased off rate allows DNA to compete with heme for binding to PhuS H209A. This is further supported by the multiple LMBs in the EMSA analysis which reflect on the kinetic competition between heme and DNA for binding to PhuS H209A during electrophoretic separation.

Previous fluorescence anisotropy (FA) assays with a 5′fluoroscein (5′-FAM) *prrF1-50* oligonucleotide confirmed the EMSA data that apo- but not holo-PhuS WT binds to the *prrF1* promoter (13). Utilizing the 5′-FAM *prrF1-50* probe (Table S2) we determined apo-PhuS H209A binds to the *prrF1* promoter with a K_D of 202 ± 60 nM a three-fold lower affinity than the PhuS WT protein (64 ± 9 nM) (Fig. 1*C*). We were unable to determine an accurate binding affinity (K_D) for holo-PhuS H209A by FA due to large variation in FA between biological replicates that we attribute to the displacement of heme interfering with FA readings.

HDX-MS analysis of the apo- and holo-PhuS H209A variant

To further understand the contribution of the conformational rearrangement and protein dynamics to the unique properties of the PhuS H209A variant we performed HDX-MS studies. Analysis of the difference in deuterium uptake for apo-*versus* holo-PhuS H209A showed a significant reduction between the two states compared to the difference in deuterium uptake of apo and holo forms of PhuS WT (Fig. 2*A*) (21). A closer examination of relative deuterium exchange in apo-PhuS H209A at the peptide level shows that it is significantly reduced compared to both the apo-PhuS WT and apo-PhuS H212R. Specifically, the C-terminal (α6/7/8) helices that form part of the heme binding pocket and provide the proximal His-209 and the alternate His-212 ligands (α7 helix), show the most dramatic loss in conformational dynamics (Fig. 3, *A* and *B*). At the earliest time point (10s), the relative deuterium uptake is ~50% for apo-PhuS WT with apo-forms of PhuS H212R and PhuS H209A showing only ~40%. Perhaps more significantly the apo-PhuS H209A shows significantly reduced rate of deuterium exchange over the time course of the experiment compared to PhuS WT and PhuS H212R (Fig. 2*A*). This is further evident on examination of the peptide encompassing the C-terminal α6-helix. Whereas the apo-PhuS WT shows a relative deuterium uptake of 50% in the α6-helix at the earliest time point (10s), apo-PhuS H212R shows only 20% and apo-PhuS H209A ~10% (Fig. 3*B*). Interestingly, at the 1 min time point where deuterium uptake by apo-PhuS WT is greater than 90%, apo-PhuS H209 A shows <30% whereas for apo-PhuS H212R the relative deuterium uptake is ~60%. Indeed, the apo-PhuS H209A never reaches 100% deuterium exchange even at the 60 min time point. This

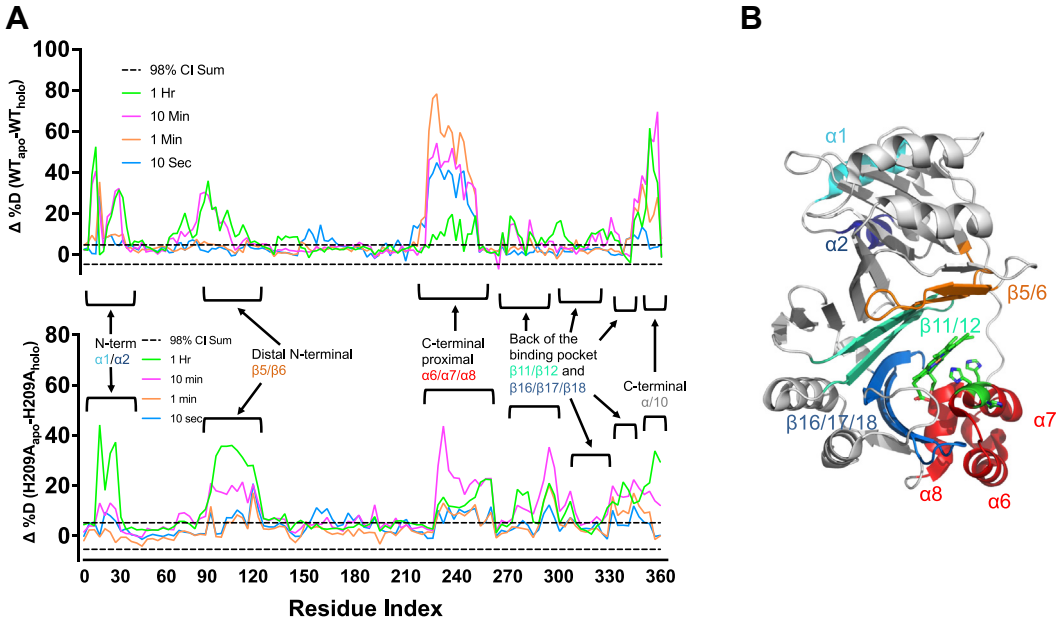

Figure 2. Difference plots of relative deuteration (Δ%D) apo-minus holo PhuS WT and PhuS H209A. (*A*) PhuS WT PhuS WT and PhuS H209A individual peptides plotted on the *x*-axis from N- to C-terminus based on the first residue number. For each peptide, differences in percentage deuteration at the various deuterium incubation times are color-coded according to the legend. Respective 98% confidence intervals (98% CIs) are represented as *horizontal dashed lines*. (*B*) holo-PhuS structure with key residues and heme shown in *stick* format. Structural domains are colored as labeled in A.

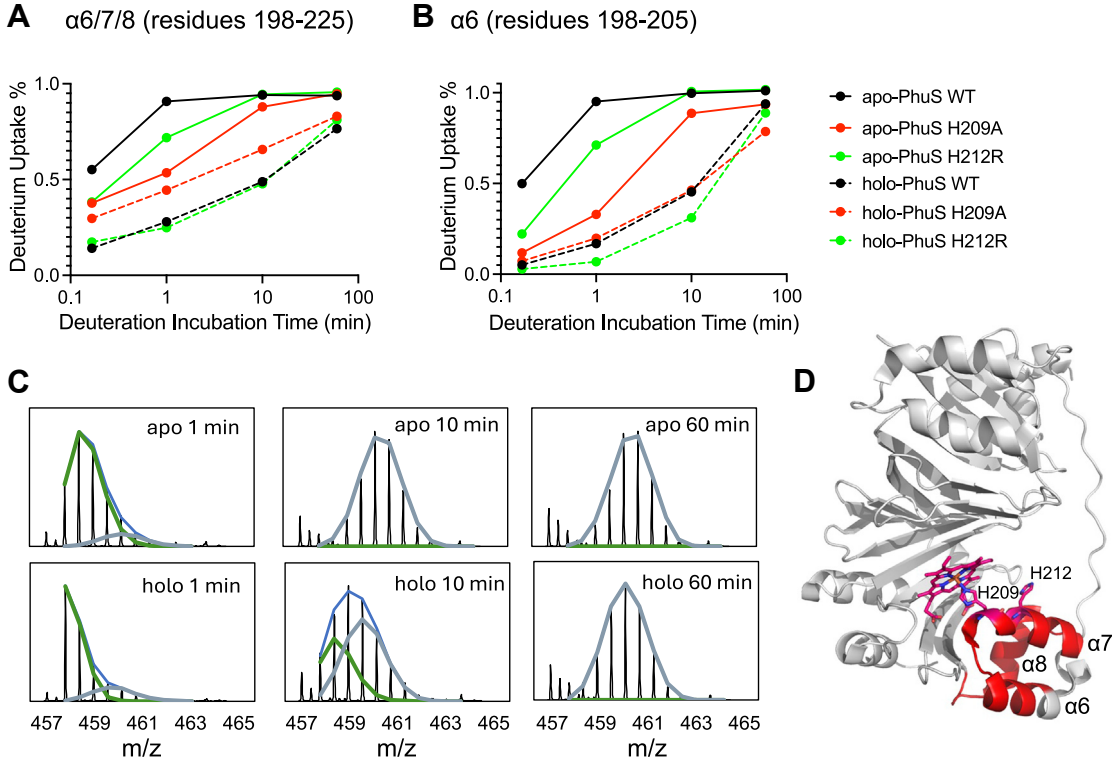

Figure 3. HDX-MS reveals differences in conformational dynamics between PhuS WT and H209A. Deuterium kinetic traces of the α6-8 (*A*) and α6 (*B*) helices as a function of time. Kinetic traces showing the relative deuteration are color coded as in the legend. % D is determined as the centroid of the isotopic envelope normalized to undeuterated and fully deuterated controls. Apo- and holo-PhuS WT and H212R data replotted from reference 21 for comparative purposes. Stacked mass spectra at 1, 10, and 60 min for apo- and holo-PhuS H209A peptides 198 to 205 (*C*) displaying instances of double-isotopic envelopes typical of EX1 kinetics. The *green* and *blue* isotopic envelopes show the change over time of distinct populations of unlabeled and labeled peptides, respectively. *D*, the holo-PhuS structure with the α6-8 and α6 helices colored *red* with heme and relevant residues in stick format. HDX-MS, hydrogen deuterium exchange coupled to mass spectrometry.

is significant as the α6-helix has been shown by combined HDX-MS and *in silico* approaches to be critical in the structural rearrangement of the C terminus on heme binding (22). The decrease in conformational flexibility in the C-terminal helices of apo-PhuS most likely arises from the fact Ala has more propensity to promote helical content than His (23). The C-terminal helices becoming successively more structured in the apo-PhuS H212R and PhuS H209A tracks with the observed changes in DNA binding where apo-PhuS H209A has the weakest affinity for the *prrF1* promoter. This would suggest that the disorder in the C-terminal helices in the absence of heme contributes to DNA binding.

The increased structural rigidity and decreased protein dynamics for apo-PhuS H209A is more evident when comparing the relative difference in deuterium exchange between the apo- and holo-forms. On heme binding to PhuS WT protein at the earliest time point (10s) there is a 50% decrease in deuterium uptake within the α6, α7, and α8 helices on heme binding, signifying a large structural and conformational rearrangement of the protein on heme binding (Fig. 3*A*). The decreased conformational flexibility for the apo-PhuS H212R shows ∼30% difference at the 10s time point. In contrast, the H209A variant shows relatively little difference with only a ∼5% decrease in deuterium uptake between the apo- and holo-states at 10s. At later time points (1 min) the apo-PhuS WT is greater than ∼90% exchanged within the α6, α7, and α8 helices whereas the holo-form is significantly protected with less than 30% exchanged (Fig. 3*A*). Similarly, the C-terminal helices for apo-PhuS H212R at the later time points (1 min) show ∼70% exchange with holo-PhuS H212R at ∼30%. The PhuS H209A protein at the 1 min time point shows the least difference between the apo- and holo-states with ∼50 and ∼40% relative exchange, respectively. This stark difference indicates that the conformational state and the degree of protection is not significantly affected by heme coordination to His-212 in the PhuS H209A variant. Perhaps not surprisingly in the C-terminal proximal α6 helix the EX1 kinetics typified by the double isotopic envelope beyond 5 min are slowed for the holo-PhuS H209A compared to holo-PhuS WT (Figs. 3*C* and S2). Interestingly, the dampening of holo-PhuS H209A EX1 kinetics extends to regions beyond the C-terminal helices that have also been shown to undergo coupled EX1 kinetics, such as the N-terminal α1,α2 helices and β5-6 sheets.

Specifically, on the distal face of the heme binding pocket, the β5-6 sheets show less difference in deuterium exchange at the earlier time points between apo- and holo-PhuS H209A than between apo- and holo-PhuS WT (Fig. 4*A*). Closer examination at the peptide level shows that the EX1 kinetics in the β5-6 sheets in the holo-PhuS H209A are similarly dampened compared to the holo-PhuS WT (Fig. 4*B* and reference

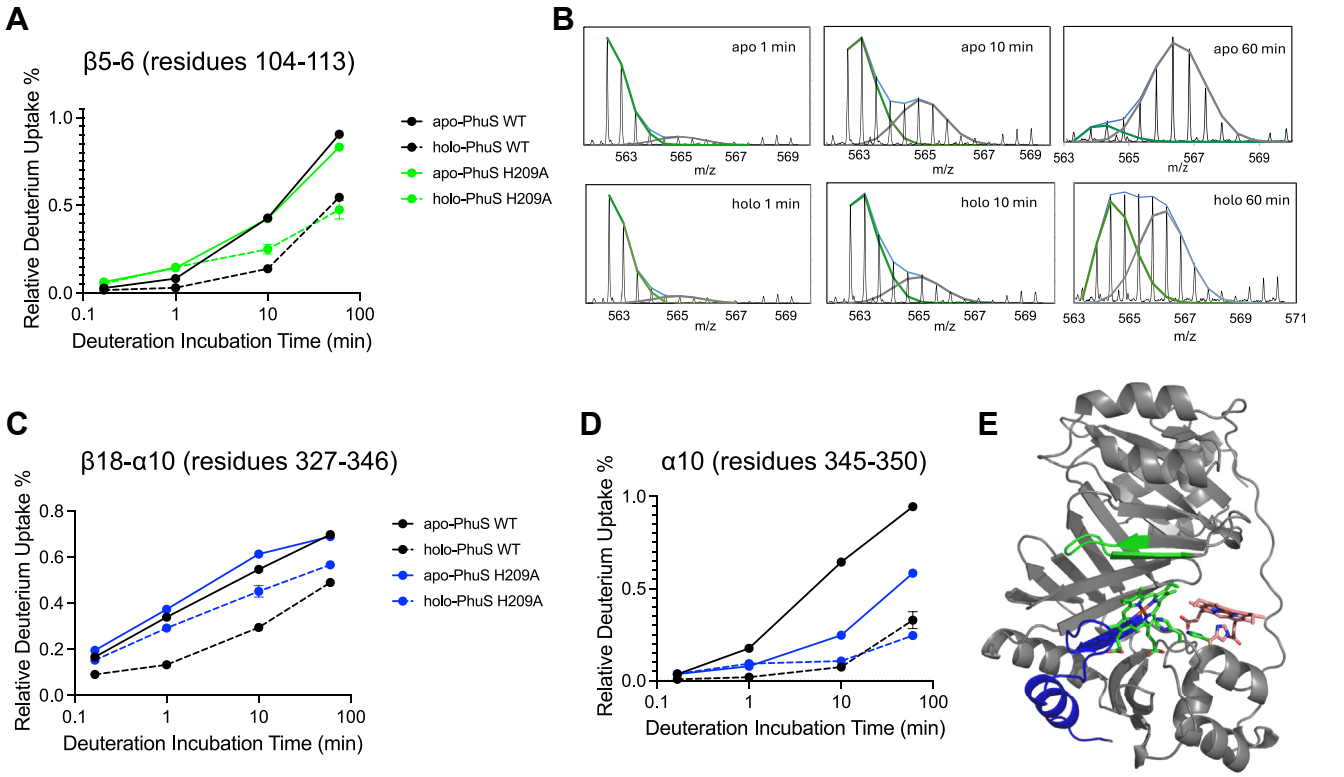

Figure 4. HDX-MS reveals differences in protection within the heme pocket between PhuS WT and H209A. Deuterium kinetic traces of the β5-6 as a function of time (*A*). Stacked mass spectra at 1, 10 and 60 min for peptides 104 to 113 (*B*) displaying instances of double-isotopic envelopes typical of EX1 kinetics. Kinetic traces of the β18-α10 (*C*) and α10 (*D*) are color coded as in the legend. The β5-6, β18-α10, and α10 are color coded as in the kinetic traces. *E*, heme coordinated through His-209 and His-212 are shown in stick format in *green* and *pink*, respectively. HDX-MS, hydrogen deuterium exchange coupled to mass spectrometry.

21). Previous modeling of heme coordination to His-212 required the His to adopt an alternate rotamer with Lys-216 and Arg-222 in position to stabilize the heme propionates (Fig. 4*E*). This alternate positioning is consistent with the decreased difference in deuterium exchange between the apo- and holo-PhuS H209A as the heme is rotated away from the β5-6 sheets toward the surface (Fig. 4*E*).

Similarly, the β18 sheet as well as the loop connecting the α10 helix at the back of the heme pocket shows significantly reduced deuterium exchange between the apo- and holo-PhuS H209A when compared to the respective PhuS WT forms (Fig. 4*C*). In the crystal structure of holo-PhuS WT, the β18 sheet and loop make direct contacts with heme coordinated through His-209 (24). However, when heme is coordinated to the protein through His-212, the proposed alternate rotamer leaves this region more exposed to the solvent (Fig. 4*E*). Similarly, the α10 helix also shows reduced differences between apo-and holo-PhuS H209A (Fig. 4*D*). However, the reduced deuterium exchange for apo-PhuS H209A compared to apo-PhuS WT suggests that the α10 helix is more structured in the PhuS H209A mutant. Taken together, the data fits with a model where heme coordination through His-212 most likely represents an intermediate on the proposed "exit from the side" transfer of heme to HemO (20, 21).

Circular dichroism of apo- and holo-H209A supports loss of heme-dependent conformational rearrangement

The HDX-MS data suggests the PhuS H209A variant adopts a more structured intermediate between the apo- and holo-PhuS WT. To further substantiate this conclusion, we performed CD on the apo- and holo-PhuS H209A compared to the WT apo- and holo-forms. The resulting spectra were analyzed and deconvoluted using the webtool BeStSel (25). In contrast to PhuS WT where there is almost a 5% increase in helicity (Fig. 5*A*) on heme binding the PhuS H209A variant shows only a 2% difference (Fig. 5*B*). The apo- and holo-PhuS H209A helical content is intermediary between the apo- and holo-PhuS WT, consistent with both states adopting conformations intermediate between the optimal conformation for DNA-binding (apo) and heme transfer (holo). The data supports our previous findings that iron coordination through His-209 drives the structural rearrangement required for the mutual exclusivity of function (21).

The phuSH209A allelic strain is compromised in regulating heme flux through HemO

Previous studies from our lab have shown the catalytic activity of HemO is required to drive heme uptake into the cell with PhuS regulating the flux of heme through HemO (10).

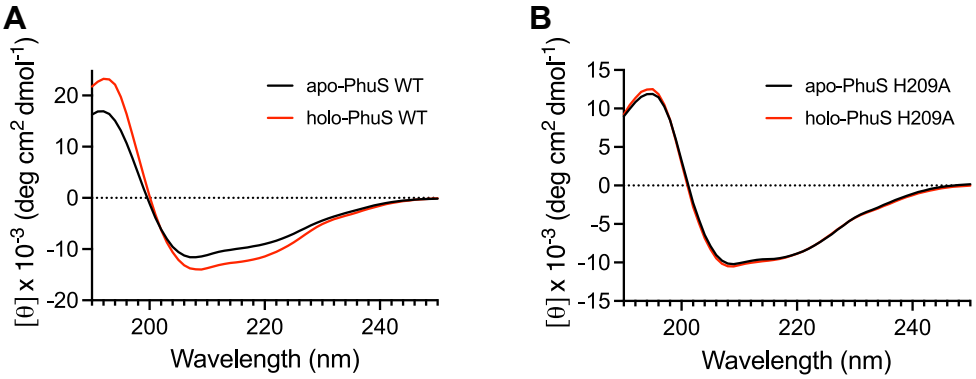

Protein	% α-helix	% β-sheet (anti-parallel)	% β-sheet (parallel)	Turn	Other
apo-PhuS H209A	18.7	16.6	7.6	11.4	45.7
holo-PhuS H209A	16.4	17.2	6.5	11.6	48.3
apo-PhuS WT	14.4	17.9	7.1	12.3	48.3
holo-PhuSWT	21.1	14.7	6.2	11.1	46.9

Figure 5. Circular dichroism of apo- and holo-PhuS WT and PhuSH209A. Spectra of PhuSWT (*A*) and PhuS H209A (*B*) were recorded in 10 mM potassium phosphate buffer (pH 7.5) at 25 °C with a final protein concentration of 10 μM.

The PhuS H209A variant has a weaker heme binding affinity (∼4-fold) and similarly the holo-PhuS shows a weaker affinity for HemO (∼6-fold) resulting in incomplete transfer of heme to HemO *in vitro* (21). To address the impact of the H209A mutation on heme transfer from PhuS to HemO *in vivo* we constructed the *phuSH209A* allelic strain. We further analyzed the protein levels of PhuS H209A in the allelic *phuSH209A* strain compared to PAO1 WT by Western blot at the 4 h time point (Fig. S3). The protein levels were significantly lower in the *phuSH209A* allelic strain compared to PAO1 WT.

We have previously shown deletion of *phuS* leads to increased metabolic flux of heme into the cell, and heme is degraded by both HemO and the alternate BVIXα selective bacterial phytochrome heme oxygenase BphO (10). BphO is encoded with a bacterial phytochrome sensor kinase in a two gene operon that is not associated with extracellular heme degradation and is not expressed under iron limiting conditions (26). Furthermore, we have shown that PhuS does not interact or transfer heme to BphO *in vitro* (9), and in the absence of HemO heme uptake into the cell is inhibited, suggesting the metabolic flux of heme into the cell is driven by the action of HemO and regulated by PhuS (10). To further determine the overall effect of the H209A mutation on the metabolic flux of heme through HemO, we utilized liquid chromatography with tandem mass spectrometry to determine the BVIX metabolite levels (12). Samples from cultures of PAO1 WT or the *phuSH209A* allelic strain were taken at 6 h following supplementation with 1 μM heme, where BVIX levels were previously shown to peak following heme supplementation (27). The BVIX levels were quantified from the resulting cell pellets. As expected, the BVIXα levels are extremely low in PAO1 WT as extracellular heme is specifically shuttled through HemO. In contrast, the *phuSH209A* allelic strain showed a significant increase in the levels of BVIXα (Fig. 6*A*). Similarly, although less significant, we observe an increase in BVIXβ and BVIXδ levels in *phuSH209A versus* PAO1 WT at the 6 h time point. The differences in BVIX metabolite profile for the *phuSH209A* strain compared to PAO1WT suggest the reduced protein levels combined with the reduced efficiency in heme transfer from holo-PhuS H209A to HemO (20), results in an uncoupling of the PhuS-HemO regulation of heme uptake. Interestingly, the BVIX metabolite profile is similar to that of the Δ*phuS* strain compared to PAO1 WT further suggesting that PhuS is critical in regulating the flux of heme into the cell (10).

The phuSH209A allelic strain shows loss of heme dependent regulation over PrrF/PrrH

To assess the impact of the H209A mutation on PrrF and PrrH, RNA levels were analyzed by quantitative polymerase chain reaction (qPCR) in low iron and 1 μM heme. The strains had similar growth rates under these conditions as previously reported for the Δ*phuS* strain (Fig. S4) (13). The PrrF probe (Table S2) detects PrrF1, PrrF2, and PrrH sRNAs due to the similarity and overlap in sequences. In contrast the PrrH probe spans the unique intergenic sequence between *prrF1* and *prrF2* and detects PrrH specifically (Table S2). Given the previously reported low abundance of PrrH compared to PrrF1 and PrrF2 (18), the contribution of PrrH to the relative RNA levels measured with the PrrF probe is negligible. We analyzed the relative mRNA levels at 2 h and 5 h where we previously

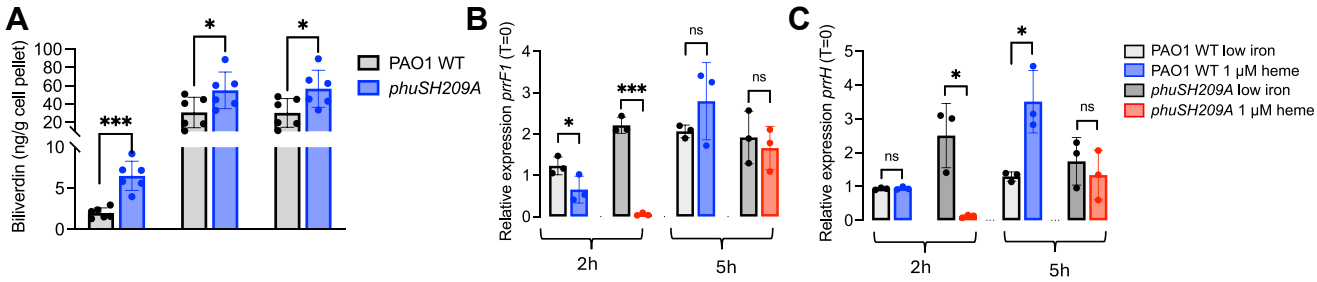

Figure 6. Quantification of the BVIX isomers and relative PrrF1 and PrrH sRNA levels in the *phusH209A* allelic strain. *A*, LC-MS/MS quantification of the BVIX isomers at 6 h following supplementation with 1 μM heme. BVIX values represent the standard deviation of six biological replicates. *p* values as determined by Student *t* test comparing the BVIXβ and BVIXδ levels isomers from the *phuSH209A* allelic strain to PAO1 WT*, $p < 0.05$ and ***, $p < 0.001$. *B*, PrrF1 relative sRNA levels for *phuSH209A* and PAO1 WT. *C*, PrrH relative sRNA levels for *phuSH209A* and PAO1 WT. mRNA isolated at 0, 2, an 5 h following growth in either iron-deplete M9 or M9 supplemented with 1 μM heme. mRNA values represent the mean from three biological experiments each performed in triplicate and normalized to 0 h. PAO1 WT data replotted from reference 13 for comparative purposes. Error bars represent the standard deviation from three independent experiments performed in triplicate for each strain. *p* values as determined by two-tailed Student *t* test comparing values following heme supplementation to iron deplete conditions at the same time point, where ***, $p < 0.001$. sRNA, small RNA; LC-MS/MS, liquid chromatography with tandem mass spectrometry.

determined heme flux is maximal and Fur repression minimal (8, 27, 28). At 2 h following heme addition, we see an initial decrease in the relative expression of PrrF due to Fur repression (Fig. 6*B*). Whereas at 5 h, the relative expression of PrrF following heme supplementation is identical to the low iron conditions. A similar heme dependent decrease in relative RNA levels at the early 2 h time point was observed for Fur regulated genes within the *has* and *phu* operons which we believe is an initial response to the influx of heme (8, 27). Interestingly, for the *phuSH209A* allelic strain the initial repression of PrrF at 2 h is greater than 10-fold (Fig. 6*C*). This is similar in the Δ*phuS* strain where increased Fur repression occurs because there is less competition for binding at the Fur box that overlaps with the PhuS binding site. While the decreased protein abundance might be expected to lead to increased Fur repression, the complete loss of heme-dependent expression over PrrH would not be expected if the protein retained its mutual exclusivity of function between the apo- and holo-form. Previous studies of a Δ*prrF1, F2* mutant indicated that one of the PrrF sRNAs had a negative effect on *phuS* expression (16). This may seem counterintuitive to the current results where repression of PrrF leads to a decrease in PhuS (Fig. 6*B*); however, it should be noted that we cannot determine by qPCR which of the PrrFs are being repressed, nor do we know which of the PrrF sRNAs is responsible for the effect on *phuS* expression. Interestingly, the *phuSH212R* strain that behaves almost identically to PAO1 WT in terms of heme transfer and has a slightly weaker DNA binding affinity (K_D), shows a two-fold reduction in PhuS protein (Fig. S5), but no Fur repression of the PrrF's, suggesting that apo-PhuS binding at the *prrF1* promoter is contributing to the relative expression of *prrF1*, *prrF2* that ultimately leads to direct feedback regulation over *phuS*. Furthermore, the loss of heme-dependence over PrrH in the *phuSH209A* strain compared to PAO1 WT (Fig. 6*C*) is consistent with the *in vitro* data where DNA displaces heme from holo-PhuS H209A (Fig. S1). Therefore, the decreased affinity of apo-PhuS H209A for the *prrF1* promoter and the loss of heme dependent regulation over PrrH contribute to the dysregulation in PrrF and PrrH expression in the *phuSH209A* allelic strain. To further analyze the role of PhuS in modulating *prrF1* and *prrF2* expression we will perform Northern blot analysis to determine their relative levels in the *phuSH209A* and *phusH212R* strain compared to PAO1 WT.

Discussion

P. aeruginosa survival within the iron-limiting environment of the host is dependent on the ability to acquire iron while maintaining iron homeostasis. This is achieved by decreasing the abundance of nonessential iron-containing proteins in iron deficient conditions. The latter process is mediated post transcriptionally by iron-responsive sRNAs that specifically target mRNAs of nonessential proteins for degradation. In *P. aeruginosa* the iron regulated PrrF sRNAs are critical for maintaining iron homeostasis while also regulating several virulence associated traits (14, 17, 29). However, it is less well understood how *P. aeruginosa* adapts to the available iron source, and how this is then integrated into adaptation within the host. Several studies have shown that in chronic infection *P. aeruginosa* adapts to utilize heme as its primary iron source at the expense of siderophore uptake (30, 31). Therefore, the ability to adapt at the transcriptional and post transcriptional level to a given iron source is critical for survival. As such apo-PhuS binding to the *prrF1* promoter as a function of Fur antagonism allows for a coordinated iron and heme transcriptional response. Moreover, differential regulation over the *prrF1* and *prrF2* promoters provides a mechanism by which the relative expression levels of PrrF1, PrrF2, and PrrH may ultimately determine the distinct target profiles of the sRNAs, especially PrrF1 and PrrF2 that have almost identical sequences. Additionally, it has been shown that the alginate regulator AlgR binds to the *prrF2* promoter (32). Thus, AlgR regulation of pyoverdine *via* PrrF2 and the PhuS heme dependent regulation over PrrF1 and PrrH may provide for differential expression of the sRNAs and hence their downstream targets.

The mutual exclusivity of PhuS as a heme chaperone *versus* transcriptional regulator hinges on the conformational

rearrangement on heme binding. Previous spectroscopic studies monitoring heme binding to PhuS showed a gradual change from free heme to holo-PhuS consistent with a two-step process (21). The initial step being formation of a noncoordinated apo-PhuS heme reversible complex driven by π-stacking hydrophobic interactions with the distal face of the heme pocket, followed by heme coordination to His-209 and conformational restructuring of the C-terminal helices. This two-step heme binding process with the initial step being the hydrophobic interaction of heme with the protein followed by a second step involving conformational rearrangement and heme coordination is conserved in many heme transport proteins including the extracellular hemophore HasAp (33). Interestingly, both apo- and holo-H209A were capable of binding to the *prrF1* promoter as judged by EMSA (Fig. 1). Interestingly, the overall difference in deuterium exchange between the apo- and holo-PhuS H209A is significantly diminished compared to the differences between the apo- and holo-states of PhuS WT suggesting that coordination to His-209 is required to drive the overall structural rearrangement and kinetic trapping of the heme. Moreover, the heme binding affinities (K_D) are in the micromolar range for PhuS WT and PhuS H209A, and the DNA binding affinities (K_D) in the nM range, supporting a kinetic locking of heme on His-209 combined with the overall conformational rearrangement that inhibits displacement by DNA. In contrast, the decrease in the heme binding affinity to PhuS H209A combined with the lack of overall conformational rearrangement when heme is coordinated through His-212 increases the kinetic lability of the heme allowing the DNA to compete off the heme.

The decreased EX1 kinetics in both the N- and C-terminal domains of holo-PhuS H209A supports a role for the cooperative folding and unfolding as being significant for function. Indeed, the loss of allosteric coupling in the N- and C-terminal domains of the PhuS H212R variant led to a decrease in heme transfer to HemO while retaining the mutual exclusivity of function between the apo- and holo-forms (13, 21). Additionally, cross-linking studies of holo-PhuS to HemO confirmed that regions shown to undergo EX-1 kinetics including the C-terminal α7/8 and N-terminal α1/2 helices are located at the protein-protein interface (21).

Based on crystallographic, spectroscopy, and cross-linking studies, we previously proposed a model for heme transfer where a ligand switch from His-209 to His-212, with His-212 adopting an alternate rotamer placing the heme in a more solvent exposed region for translocation to HemO (21). The HDX-MS analysis of PhuS H209A is consistent with this model where the holo-PhuS H209A coordination through His-212 is a transition state intermediate between heme delivery and subsequent release from HemO. As such heme binding to His-212 in the PhuS H209A variant does little to drive the significant conformational rearrangement required for the mutual exclusivity of function between the apo- and holo-state. This can be seen at the peptide level where the HDX-MS profiles of the apo- and holo-PhuS H209A within the N- and C-terminal helices are more similar to each other than the respective apo- and holo-PhuS WT states (Figs. 2 and 3). Therefore, taken together the overall structural rearrangement afforded by the coordination of the heme iron by His-209, combined with the allosteric folding and unfolding within regions of the N- and C-terminus, are required for optimal conformational rearrangement and heme transfer, respectively.

Additionally, the decreased protein abundance as well as the weaker binding affinity for HemO leads to reduced efficiency of heme transfer to HemO. The effect of uncoupling PhuS and HemO, as in the Δ*phuS* strain, leads to an increase in heme flux through HemO and increased BVIXβ and BVIXδ levels. As previously reported PhuS acts as a specific heme titratable regulator of heme flux through HemO and either loss of or a decreased ability to traffic heme to HemO leads to dysregulation of extracellular heme metabolism (10). Moreover, the loss of regulation of heme uptake has significance not only in the potential for heme toxicity but the fact that BVIXβ is a signaling molecule. Specifically, we have shown BVIXβ post-transcriptionally upregulates HasAp allowing *P. aeruginosa* to rapidly respond to extracellular heme levels *via* the heme metabolites (8, 27). Furthermore, we have recently shown BVIXβ functions as a chemotactic and signaling molecule integrating the utilization of heme as an iron source into the regulatory and chemosensory systems associated with adaptation from a planktonic to sessile lifestyle (12). Thus, the disruption of the metabolic flux of the heme through the PhuS-HemO couple has significant ramifications in terms of iron-homeostasis and adaptation within the host environment. Therefore, PhuS is a central player linking heme metabolism and iron-homeostasis with *P. aeruginosa's* adaptation to its environment, and as such represents a viable therapeutic target for the development of new antibiotics.

Experimental procedures

Bacterial strains and growth conditions

All bacterial strains, plasmids, and oligonucleotides used in this study are listed in Tables S1 and S2. All primers and probes used in this study were purchased from Integrated DNA Technologies (IDT). *Escherichia coli* strains were routinely grown in Luria Bertani (LB) broth (Invitrogen) or on LB-agar plates. *P. aeruginosa* strains were always freshly streaked and maintained on *Pseudomonas* isolation agar (PIA) (BD Biosciences). All bacterial strains were stored in at −80 °C in LB broth with 20% glycerol. The iron levels in M9 medium (Nalgene) were determined by inductively coupled plasma-mass spectrometry to be less than 1 nM. For all experiments, *P. aeruginosa* colonies were isolated freshly streaked PIA plates. Single colonies were selected to inoculate 5 ml of LB (n = 3–6) and grown at 37 °C with shaking for 8 to 16 h. The cells were pelleted by centrifugation and resuspended in 2 ml M9 minimal media. Cells were centrifuged and resuspended a further two times in M9 before resuspending in 10 to 50 ml of M9 minimal media. For all experiments cultures were inoculated to a final A_{600} of 0.04. Cultures were grown at 37 °C with shaking for 3 h before the addition of supplements (0 h) and incubated for a further 2 to 8 h depending on the specific

experiments. For growth curves, 200 µl of cultures supplemented with or without 1 µM heme were aliquoted into clear 96-well plates. Cultures were then incubated in a BioTek Synergy HT plate reader at 37 °C with shaking for 18 h and the A_{600} measured every half hour. Data were collected for four biological replicates and three technical replicates, and results were plotted in GraphPad Prism. When required, antibiotics were used at the following final concentrations tetracycline (Tc) 10 and 150 µg ml^{-1} for *E. coli* and *P. aeruginosa*, respectively. Ampicillin (Amp) for purposes of protein expression in *E. coli* was used at a final concentration of 100 µg/ml.

Gene expression analysis by quantitative real time PCR

For qPCR experiments, 50 ml iron-depleted cultures were supplemented with or without 1 µM heme and grown at 37 °C and 1 ml aliquots collected at 2 h and 5 h. RNA was stabilized by the addition of 250 µl RNAlater Solution (Ambion), and the samples were stored at −80 °C until further use. Total RNA was isolated from each cell pellet using the RNAeasy mini spin columns according to the manufacturer's directions (Qiagen). Subsequently, 6 µg of total RNA was treated with RNAse-free *DNAse*I (New England Biolabs) for 2 h at 37 °C to remove contaminating chromosomal DNA and precipitated with 0.1x volume 3M sodium acetate pH 5.2 and 2x volume 100% (v/v) ethanol. RNA quantity and quality were assessed by UV absorption at 260 nm in a NanoDrop 2000c Spectrophotometer (Thermo Fisher Scientific). Complementary DNA (cDNA) was generated using the GoScript Reverse Transcriptase kit (Promega) from RNA (250 ng) and random primers (0.5 µg). cDNA (10 ng) was analyzed with gene specific primers (Table S2) using the StepOnePlus Real-Time PCR System (Applied Biosystems) and FastStart Universal Probe Master (Rox) (Roche). The relative gene expression was calculated using the ΔΔ*Ct* method and the cycle threshold (*Ct*) values at each time point were normalized to the constitutively expressed *23S* gene. mRNA values represent the standard deviation of three independent experiments performed in triplicate.

Construction of the P. aeruginosa *phuSH209A* allelic strain

phuSH209A was obtained by allelic exchange as previously described for the *phuSH212R* allelic strain (13), using the parental strain PAO1 Δ*phuS* (34). Briefly, a 2.9 kb *phuS* gene fragment including upstream and downstream sequence was PCR amplified from the chromosomal DNA of *P. aeruginosa PAO1* using primers pairs *Pst*I-5′PhuS-F and HindIII-3′PhuS-R. The amplified fragment was cloned into pUC18, resulting in pUC18-5′-PhuS-3′. The mutant allele *phuSH209A* was obtained following digestion of plasmid pET21*phuSH209A* (21) with NruI and StuI and subcloned into NruI and StuI digested pUC18-5′-PhuS-3′, replacing the WT allele. The new construct pUC18-5′-*phuS*H209A-3′ was confirmed by sequencing (Eurofins MWG Operon). The insert including *phuS*H209A plus the 5′ and 3′ flanking regions was purified by PstI-HindIII digestion and ligated into the counter-selective suicide plasmid pEX18Tc (35). Finally, plasmid pEX18Tc-5′-*phuSH209A*-3′ was transferred into *P. aeruginosa* Δ*phuS* by conjugation. A double event of homologous recombination followed by selection on PIA plates containing 5% sucrose, resulted in chromosomal integration of *phuSH209A*, replacing the parental allele Δ*phuS*. PCR and DNA sequencing analysis were used to verify the allelic exchange process.

Expression and purification of apo-PhuS and PhuSH209A

Protein expression was performed as previously reported with minor modification (9, 20). The PhuS or PhuS H209A mutant lysate was applied to a Sepharose-G column (GE Life Sciences) equilibrated with 20 mM Tris–HCl (pH 8.0) and 20 mM NaCl and washed with five column volumes of the same buffer. The column was further washed with 10 column volumes of 20 mM Tris (pH 8.0) containing 20 mM NaCl and the PhuS protein eluted with a linear gradient of 20 to 400 mM NaCl. Eluted fractions were analyzed by SDS-PAGE, and the peak fractions pooled and dialyzed against 4 L of 20 mM Tris (pH 8.0) containing100 mM NaCl. The protein was concentrated in a Pierce Protein Concentrators (30K) (Thermo Fisher Scientific) and purified to homogeneity on an AKTA FPLC system fitted with a 26/60 Superdex 200 pg size-exclusion column (GE Life Sciences) equilibrated with 20 mM Tris (pH 8.0) containing 100 mM NaCl. Peak fractions as judged by the A_{280} were subjected to SDS-PAGE and the pure fractions pooled, concentrated (10 mg/ml), and stored at −80 °C until further use.

Heme solutions were prepared in 0.1 N NaOH, and the pH adjusted with the identical buffer used to prepare the PhuS protein samples. Heme loading of the purified PhuS protein was carried out by addition of a 1.5:1 ratio of heme to protein. Excess heme was removed over a Sephadex G-50 column (GE Life Sciences) equilibrated with 20 mM Tris (pH 8.0). All buffered heme solutions were used within 20 min of preparation. Heme stock solution concentrations and the stoichiometry of the final holo-PhuS complexes were determined by pyridine hemochrome as previously described (36).

Western blot analysis

Aliquots from cultures supplemented with 1 µM heme were collected at the 4, 6, and 8 h centrifuged at 5000 rpm for 10 min at 4 °C. Pellets were lysed in 250 µl of BugBuster HT Protein Extraction Reagent (Millipore Sigma) containing 1x Halt protease inhibitor and incubated at room temperature on a rotating platform for 20 min and then spun down and collected in a fresh Eppendorf tube. Total protein concentrations were determined using the Bio-Rad reducing agent compatible and detergent compatible assay Samples of the cell lysate (10 mg of total protein) and Chameleon duo prestained protein ladder in 4X protein sample loading buffer (LI-COR) were run on a 12% SDS-PAGE. Proteins were transferred by electrophoresis to low fluorescence polyvinylidene difluoride membrane (Bio-Rad) for Western blot analysis. Membranes were then stained with Revert 700 Total Protein Stain (LI-COR) to measure the total protein levels on the 700 nm

channel of the Odyssey M (LI-COR) imaging system. Stained membranes were destained with Revert Destaining Solution (LI-COR) prior to imaging. The membranes were then blocked with blocking buffer (5% w/v skim milk in Tris-buffered saline (TBS) with 0.1% v/v Tween 20), washed, and probed with a 1:2500 dilution of anti-PhuS primary antibodies (13) in hybridization buffer (1% w/skim milk in TBS with 0.2% v/v Tween 20). Membranes were rinsed three times in TBS with 0.2% (v/v) Tween 20 and probed with IRDye 800CW Goat Anti-Rabbit IgG (LI-COR) at a dilution of 1:25,000 in hybridization buffer. Proteins were visualized on the 800 nm channel of the Odyssey M (LI-COR) imaging system. Quantitation of PhuS intensity normalized to total protein was performed using the Empiria Studio Software package. All experiments are performed on four biological replicates per strain and statistically analyzed by Student's *t* test.

Hydrogen deuterium exchange coupled to mass spectrometry

Firstly, undeuterated controls were prepared to obtain the peptide coverage map for apo-PhuS (Fig. S5). The experimental workflow was as follows: 2 µl of 20 µM apo-PhuS in 50 mM Tris pH 7.5, 150 mM NaCl was diluted with 18 µl of 50 mM Tris pH 7.5, 150 mM NaCl, then 50 µl of ice-cold quench was added (100 mM glycine pH 2.5, 8 M Urea, and 500 mM TCEP) followed by 180 µl of 100 mM glycine buffer pH 2.5. The 250 µl dilution was injected into a Waters HDX technology (Waters) equipped with an M-class UPLC and an in-line manually packed column using pepsin bead slurry from Thermo Fisher Scientific. Peptic fragments were trapped on an ACQUITY UPLC BEH C18 peptide trap and separated on an ACQUITY UPLC BEH C18 column. A 7 min, 5% to 35% acetonitrile in 0.1% formic acid gradient was used to elute the peptides directly into a Waters Synapt G2-Si mass spectrometer (Waters). Mass spectrometry (MS) data were acquired with a 20 to 30 V ramp trap collision energy for high energy acquisition of product ions and continuous lock mass (Leucine-Enkephalin) for correction of mass accuracy. Peptides were identified using the ProteinLynx Global Server 3.0.3 (Waters). A filter of 0.3 fragments per residue was applied for peptide processing in the DynamX 3.0 software (Waters).

Hydrogen-deuterium exchange reactions for apo-PhuS and holo-PhuS were performed by manual injections. The reaction workflow for manual injections was as follows for the apo-protein: 2 µl of 20 µM apo-PhuS in 50 mM Tris pH 7.5, 150 mM NaCl was diluted with 18 µl of 50 mM Tris pH 7.5, 150 mM NaCl in D_2O (99.99%), pD 7.5. The 20 µl reaction was quenched at various time points with 50 µl of ice-cold quench (100 mM glycine pH 2.5, 8 M Urea, 500 mM TCEP) followed by addition of 180 µl of ice-cold 100 mM glycine buffer, pH 2.5. All the deuteration reactions were carried out at 25 ℃ at four reaction time points (10 s, 1 min, 10 min, and 1 h). Following quenching of the deuterated samples, the 250 µl total reaction was injected and LC/MS acquisition was performed in the same manner as the undeuterated controls. The four deuteration time points were acquired in triplicate. Fully deuterated controls were performed for normalization purposes. The normalized percent deuterium uptake (% D) for each peptide, at incubation time *t*, was calculated from the following equation:

$$\%\, D = \frac{100 \times (m_t - m_0)}{m_f - m_0}$$

Circular dichroism

CD spectra of apo-PhuS H209A and holo-PhuS H209A were acquired using a JASCO J-1500 CD Spectrophotometer. All samples were recorded in 10 mM potassium phosphate (pH 7.5) at 25 °C from 190 to 250 nm, with a data pitch of 0.5 nm and a protein concentration of 5 µM. The molar ellipticity was calculated directly from the JASCO SpectraManager software, and then converted to mean residue ellipticity for data analysis purposes. The resulting spectra were deconvoluted using the BeStSel webtool to estimate the secondary structure and differences in percent helicity between apo- and holo-PhuS H209A (25).

Electrophoretic mobility shift assay

Double stranded 5′-biotin-labeled oligonucleotides were purchased from Integrated DNA Technologies (IDT) and reconstituted in DNase/RNase free water (Table S2). DNA concentration was determined from the absorption at 260 nm in a NanoDrop One^C spectrophotometer. All protein oligonucleotide binding reactions contained a final concentration of 20 mM Tris, 100 mM NaCl, 10% glycerol, and 0.2 ng/ml salmon sperm DNA. Apo- and holo-PhuS H209A protein concentrations ranged from 0.1 µM to 20 µM. All reactions were incubated at 37 °C for 20 min before the addition of the biotinylated probes. For all reactions, the oligonucleotide probes were used at a fixed concentration of 30 pM in a final reaction volume of 10 µl. Following addition of the probes, the reactions were incubated at 37 °C for a further 20 min and analyzed on a 10% Tris-Glycine gel (Bio-Rad). The gel was prerun in 1X Tris-Glycine buffer (pH 8.3) for 1 h at 200 V 4 °C and following sample loading a further 2 h at same voltage. The protein–DNA complex was then transferred to a positively charged nylon membrane (BrightStar Plus Nylon Membrane; Invitrogen) using a semiwet electroblotting transfer system with 1x Tris-Glycine (pH 8.5) for 30 min at 30 mA. Membranes were washed in 2X saline-sodium citrate buffer (Thermo Fisher Scientific), for 5 min at room temperature, and DNA immobilized by UV crosslinking. The position of the DNA was visualized by chemiluminescent detection using the Chemiluminescent Nucleic Acid Detection Module (Thermo Fisher Scientific) as directed by the manufacturer and exposed to X-ray film (Amersham hyperfilm ECL; Amersham).

Quantification of the BVIX isomers

Sample collection and quantitation were performed as previously described (12). Briefly, shaken culture samples were collected by centrifugation at 4, 6, and 8 h. Pellets were

resuspended to yield a final concentration of 1 mg/μl concentration (50 μl of resuspension buffer to 50 mg of pellet) and then combined at a 1:40 ratio with 200 μM butylated hydroxytoluene (BHT), and then 25 μl of the resuspended pellet was combined with 975 μl of 200 μM BHT in acetonitrile:water/1:1 (v/v). Subsequently, 10 μl of 50 ng/ml BVIXα-d4 (Sigma-Aldrich) was added to each sample as an internal standard. The resulting solution was acidified with 100 μl of 1 N HCl followed by a liquid-liquid extraction using 1.5 ml of ethyl acetate. Samples were briefly vortexed and then centrifuged at 4 °C for 10 min at 3000 rpm. Using a dry-ice bath, the bottom (aqueous) layer was frozen, and the top (organic) layer was decanted into a new test tube. This step helped to minimize variable recovery due to emulsions. Samples were dried at ambient temperature under nitrogen gas (∼25 min) and then reconstituted with 100 μl of 200 μM BHT in acetonitrile:water/1:1 (v/v). We found that BHT is a necessary addition as an antioxidant to prevent nonspecific oxidation of residual heme in samples since excreted metabolites can facilitate redox reactions.

Samples were analyzed using an I Class UPLC coupled to a TQ-XS triple quadrupole mass spectrometer (Waters Corporation) using the previously published MS parameters (12). An Acentis 90 Å RP Amide Column, 100 mm × 2.1 mm, 2.7 μm was used for chromatographic separation using a gradient separation with mobile phase A as 0.1% formic acid in water and mobile phase B as 0.1% formic acid in acetonitrile. The gradient separation started at 35% B and was held for 2 min, ramped to 45 % B over 2 min, ramped to 95% B over 2.5 min, and then returned to 35% B for a total analytical run time of 10 min.

SEC of the holo-PhuSH209A-DNA complex

SEC was performed on an AKTA chromatography instrument (Cytiva) fitted with a Superdex 200 increase 10/300 GL column (Cytiva). Holo-PhuS H209A was made fresh as previously described in this methods section, and double stranded unlabeled PrrF1 promoter was made fresh in annealing buffer (10 mM Tris/150 mM NaCl/1 mM EDTA). For the protein–DNA complex holo-H209A was incubated for 20 min at 37 °C with an equimolar concentration of the PrrF promoter (P_{prrF1}) at a final concentration of 4.7 μM. Holo-H209A without DNA and P_{prrF1} without protein were mixed with autoclaved deionized water to a concentration of 4.7 μM and incubated at 37 °C for 20 min. Samples were analyzed on a Superdex Increase 5/150 GL (Cytiva) previously equilibrated in 20 mM Tris/150 mM NaCl with a flow rate of 0.75 ml/min. The absorption was monitored at 260 nm, 280 nm, and 400 nm wavelengths for the DNA, protein and heme, respectively. All runs were performed at 4 °C and all data collected using the UNICORN 7.6 software and exported for analysis in Prism GraphPad version 10.

Quantitative Real-Time PCR

To analyze *prrF* or prrH expression, singly isolated colonies of *P. aeruginos*a parental strain or the *phuSH209A* allelic strain were picked, inoculated into 10 ml of LB broth, and grown overnight at 37 °C with shaking (210 rpm). The bacteria were then harvested and washed in 10 ml of M9 minimal medium. Following centrifugation, the bacterial pellet was resuspended in 10 ml of M9 medium and used to inoculate 50 ml of fresh M9 iron-deplete medium to a starting A_{600} of 0.05. Cultures were grown at 37 °C with shaking for 3 h before the addition of 1 μM heme (0 h) and incubated for a further 7 h. Total RNA was purified from 1 to 2 ml aliquots collected at several time points from cultures grown under various conditions (with and without 1 μM heme). RNA was stabilized by the addition of 250 μl RNAlater Solution (Ambion) and the samples were stored at −80 °C until further use. Total RNA was isolated from each cell pellet using the RNAeasy mini spin columns according to the manufacturer's directions (Qiagen). In addition, 4 μg of total RNA was treated with RNAse-free DNAse I (New England Biolabs) for 2 h at 37 °C to remove contaminating chromosomal DNA and precipitated with 0.1x volume 3M sodium acetate pH 5.2 and 2x volume 100% (v/v) ethanol. RNA quantity and quality were assessed by UV absorption at 260 nm in a NanoDrop 2000c Spectrophotometer (Thermo Fisher Scientific). cDNA was generated using the GoScript Reverse Transcriptase kit (Promega) from RNA (250 ng) and random primers (0.5 μg). cDNA (10 ng) was analyzed with gene specific primers (Table S2) using the StepOnePlus Real-Time PCR System (Applied Biosystems) and FastStart Universal Probe Master. The relative gene expression was calculated using the ΔΔCt method and the cycle threshold (180) values at each time point were normalized to the constitutively expressed 23S gene. mRNA values represent the standard deviation of three independent experiments performed in triplicate.

Fluorescence anisotropy

FA experiments were performed as previously described (13). Briefly, 5′-FAM oligonucleotides of the protected *prrF1* promoter region (Table S2) were analyzed by UV–visible spectroscopy to quantify the percentage of fluorescein tag. The double-stranded probe was obtained by combining a 1:1 ratio of the 5′-labeled sense and unlabeled antisense oligonucleotides in deionized annealing buffer (10 mM Tris/150 mM NaCl/1 mM EDTA). To facilitate annealing, mixtures were heated to 95 °C, 5 min, and cooled down to room temperature. The labeled double-stranded oligonucleotides were stored at −80 °C until further use. In a quartz cuvette, 10 nM of 5′-FAM oligonucleotide was diluted in 20 mM Tris–HCl (pH 8.0), containing 100 mM NaCl, and 0.05 mg/ml bovine serum albumin in a final volume of 500 μl. For binding studies with Fur, 10 nM of 5′-FAM oligonucleotide was diluted in 10 mM bis–Tris borate (pH 7.5), 40 mM KCl, 0.1 mM MnSO4, 0.1 mg/ml bovine serum albumin, and 10% glycerol. All measurements were performed on a K2 spectrofluorometer (ISS) configured in the L-format, with excitation/emission wavelengths and band widths of 495 and 2 nm and 519 and 1 nm, respectively. A measurement of the maximum anisotropy was performed on the 5′-FAM oligonucleotides, and the

change in anisotropy was measured as a function of increasing concentrations of PhuS or Fur. The addition of protein continued until no further change in anisotropy was observed. The data were fit by converting the anisotropy, *r*, to fraction bound, F_{bound} (the fraction of protein bound to the oligonucleotide at a given DNA concentration), using the following equation:

$$Fbound = r - \frac{rfree}{(rbound - r)Q + (r - rfree)}$$

where r_{free} is the anisotropy of the fluorescein-labeled oligonucleotide and r_{bound} is the anisotropy of the oligonucleotide–protein complex at saturation. The quantum yield designated as Q is calculated from the changes in fluorescence intensity that occurs over the course of the experiment (I_{bound}/I_{free}). F_{bound} was then plotted against the protein concentration using a one-site binding model:

$$P + D \leftrightarrow PD \frac{[P][D]}{[PD]} = K_d$$

$$F_{bound} = \{P_{total} + D_{total} + K_d) - \frac{\left[\left(\sqrt[2]{P_{total}+D_{total}+K_d)} - 4P_{total}D_{total}\right)_{1/2}\right]}{2D_{total}}$$

where P is the protein concentration and D is the DNA concentration. All concentrations and fluorescence changes were done in triplicate and corrected for volume changes.

Data availability

All data are presented in the manuscript.

Supporting information—This article contains supporting information.(9,13,21,34,35,37)

Author contributions—N. M., T. W., S. A. K., S. M., M. A. K., D. D., and A. W. investigation; N. M., T. W., S. A. K., S. M., and A. W. data curation; N. M., T. W., S. A. K., S. M., M. A. K., D. D., and A. W. writing–review and editing; N. M., T. W., M. A. K., D. D., and A. W. conceptualization; N. M., T. W., D. D., and A. W. validation; N. M., S. A. K., S. M., M. A. K., D. D., and A. W. formal analysis; N. M. and A. W. writing–original draft; N. M. visualization; S. A. K. and A. W. methodology; M. A. K., D. D., and A. W. supervision; M. A. K., D. D., and A. W. resources; A. W. project administration; A. W. funding acquisition.

Funding and additional information—This research was funded by National Institutes of Health grant R01AI161294 to A. W. and Research Diversity supplement R01AI161294-S to N. M. The content is solely the responsibility of the authors and does not necessarily represent the official views of the National Institutes of Health."

Conflict of interests—The authors declare that they have no conflicts of interest with the contents of this article.

Abbreviations—The abbreviations used are: BHT, butylated hydroxytoluene; BV, biliverdin; FA, fluorescence anisotropy; Fur, ferric uptake regulator; Has, heme assimilation system; HDX-MS, hydrogen deuterium exchange coupled to mass spectrometry; HemO, heme oxygenase; LMB, lower mobility band; MS, mass spectrometry; Phu, *Pseudomonas* heme uptake; PIA, *Pseudomonas* isolation agar; qPCR, quantitative polymerase chain reaction; SEC, size-exclusion chromatography; TBS, Tris-buffered saline.

References

1. Johnson, E. E., and Wessling-Resnick, M. (2012) Iron metabolism and the innate immune response to infection. *Microbe. Infect.* **14**, 207–216
2. Hood, M. I., and Skaar, E. P. (2012) Nutritional immunity: transition metals at the pathogen-host interface. *Nat. Rev. Microbiol.* **10**, 525–537
3. Contreras, H., Chim, N., Credali, A., and Goulding, C. W. (2014) Heme uptake in bacterial pathogens. *Curr. Opin. Chem. Biol.* **19**, 34–41
4. Huang, W., and Wilks, A. (2017) Extracellular heme uptake and the challenge of bacterial cell membranes. *Annu. Rev. Biochem.* **86**, 799–823
5. Murdoch, C. C., and Skaar, E. P. (2022) Nutritional immunity: the battle for nutrient metals at the host-pathogen interface. *Nat. Rev. Microbiol.* **20**, 657–670
6. Ochsner, U. A., Johnson, Z., and Vasil, M. L. (2000) Genetics and regulation of two distinct haem-uptake systems, *phu* and *has*, in *Pseudomonas aeruginosa*. *Microbiology* **146**, 185–198
7. Smith, A. D., and Wilks, A. (2015) Differential contributions of the outer membrane receptors PhuR and HasR to heme acquisition in *Pseudomonas aeruginosa*. *J. Biol. Chem.* **290**, 7756–7766
8. Dent, A. T., Mourino, S., Huang, W., and Wilks, A. (2019) Post-transcriptional regulation of the *Pseudomonas aeruginosa* heme assimilation system (Has) fine-tunes extracellular heme sensing. *J. Biol. Chem.* **294**, 2771–2785
9. Lansky, I. B., Lukat-Rodgers, G. S., Block, D., Rodgers, K. R., Ratliff, M., and Wilks, A. (2006) The cytoplasmic heme-binding protein (PhuS) from the heme uptake system of *Pseudomonas aeruginosa* is an intracellular heme-trafficking protein to the delta-regioselective heme oxygenase. *J. Biol. Chem.* **281**, 13652–13662
10. O'Neill, M. J., and Wilks, A. (2013) The *P. aeruginosa* heme binding protein PhuS is a heme oxygenase titratable regulator of heme uptake. *ACS Chem. Biol.* **8**, 1794–1802
11. Ratliff, M., Zhu, W., Deshmukh, R., Wilks, A., and Stojiljkovic, I. (2001) Homologues of neisserial heme oxygenase in gram-negative bacteria: degradation of heme by the product of the *pigA* gene of *Pseudomonas aeruginosa*. *J. Bacteriol.* **183**, 6394–6403
12. Shahzad, S., Krug, S. A., Mourino, S., Huang, W., Kane, M. A., and Wilks, A. (2024) *Pseudomonas aeruginosa* heme metabolites biliverdin IXbeta and IXdelta are integral to lifestyle adaptations associated with chronic infection. *mBio* **15**, e0276323
13. Wilson, T., Mourino, S., and Wilks, A. (2021) The heme binding protein PhuS transcriptionally regulates the *Pseudomonas aeruginosa* tandem sRNA *prrF1,F2* locus. *J. Biol. Chem.* **296**, e100275
14. Wilderman, P. J., Sowa, N. A., FitzGerald, D. J., FitzGerald, P. C., Gottesman, S., Ochsner, U. A., *et al.* (2004) Identification of tandem duplicate regulatory small RNAs in *Pseudomonas aeruginosa* involved in iron homeostasis. *Proc. Natl. Acad. Sci. U. S. A* **101**, 9792–9797
15. Oglesby, A. G., Farrow, J. M., 3rd, Lee, J. H., Tomaras, A. P., Greenberg, E. P., Pesci, E. C., *et al.* (2008) The influence of iron on *Pseudomonas aeruginosa* physiology: a regulatory link between iron and quorum sensing. *J. Biol. Chem.* **283**, 15558–15567
16. Reinhart, A. A., Powell, D. A., Nguyen, A. T., O'Neill, M., Djapgne, L., Wilks, A., *et al.* (2015) The *prrF*-encoded small regulatory RNAs are required for iron homeostasis and virulence of *Pseudomonas aeruginosa*. *Infect. Immun.* **83**, 863–875
17. Nelson, C. E., Huang, W., Brewer, L. K., Nguyen, A. T., Kane, M. A., Wilks, A., *et al.* (2019) Proteomic analysis of the Pseudomonas aeruginosa

iron starvation response reveals PrrF small regulatory RNA-dependent iron regulation of twitching motility, amino acid metabolism, and zinc homeostasis proteins. *J. Bacteriol.* **201**, e00754
18. Oglesby-Sherrouse, A. G., and Vasil, M. L. (2010) Characterization of a heme-regulated non-coding RNA encoded by the *prrF* locus of *Pseudomonas aeruginosa*. *PLoS One* **5**, e9930
19. Reinhart, A. A., Nguyen, A. T., Brewer, L. K., Bevere, J., Jones, J. W., Kane, M. A., *et al.* (2017) The *Pseudomonas aeruginosa* PrrF small RNAs regulate iron homeostasis during acute murine lung infection. *Infect. Immun.* **85**, e00764
20. O'Neill, M. J., Bhakta, M. N., Fleming, K. G., and Wilks, A. (2012) Induced fit on heme binding to the *Pseudomonas aeruginosa* cytoplasmic protein (PhuS) drives interaction with heme oxygenase (HemO). *Proc. Natl. Acad. Sci. U. S. A* **109**, 5639–5644
21. Deredge, D. J., Huang, W., Hui, C., Matsumura, H., Yue, Z., Moenne-Loccoz, P., *et al.* (2017) Ligand-induced allostery in the interaction of the *Pseudomonas aeruginosa* heme binding protein with heme oxygenase. *Proc. Natl. Acad. Sci. U. S. A* **114**, 3421–3426
22. Kihn, K. C., Wilson, T., Smith, A. K., Bradshaw, R. T., Wintrode, P. L., Forrest, L. R., *et al.* (2021) Modeling the native ensemble of PhuS using enhanced sampling MD and HDX-ensemble reweighting. *Biophys. J.* **120**, 5141–5157
23. Chakrabartty, A., Kortemme, T., and Baldwin, R. L. (1994) Helix propensities of the amino acids measured in alanine-based peptides without helix-stabilizing side-chain interactions. *Protein Sci.* **3**, 843–852
24. Tripathi, S., O'Neill, M. J., Wilks, A., and Poulos, T. L. (2013) Crystal structure of the *Pseudomonas aeruginosa* cytoplasmic heme binding protein, Apo-PhuS. *J. Inorg. Biochem.* **128**, 131–136
25. Micsonai, A., Moussong, E., Wien, F., Boros, E., Vadaszi, H., Murvai, N., *et al.* (2022) BeStSel: webserver for secondary structure and fold prediction for protein CD spectroscopy. *Nucleic Acids Res.* **50**, W90–W98
26. Wegele, R., Tasler, R., Zeng, Y., Rivera, M., and Frankenberg-Dinkel, N. (2004) The heme oxygenase(s)-phytochrome system of *Pseudomonas aeruginosa*. *J. Biol. Chem.* **279**, 45791–45802
27. Mourino, S., Giardina, B. J., Reyes-Caballero, H., and Wilks, A. (2016) Metabolite-driven regulation of heme uptake by the biliverdin IXbeta/delta-selective heme oxygenase (HemO) of *Pseudomonas aeruginosa*. *J. Biol. Chem.* **291**, 20503–20515
28. Dent, A. T., and Wilks, A. (2020) Contributions of the heme coordinating ligands of the *Pseudomonas aeruginosa* outer membrane receptor HasR to extracellular heme sensing and transport. *J. Biol. Chem.* **295**, 10456–10467
29. Hoang, T. M., Huang, W., Gans, J., Weiner, J., Nowak, E., Barbier, M., *et al.* (2023) The heme-responsive PrrH sRNA regulates *Pseudomonas aeruginosa* pyochelin gene expression. *mSphere* **8**, e0039223
30. Marvig, R. L., Damkiaer, S., Khademi, S. M., Markussen, T. M., Molin, S., and Jelsbak, L. (2014) Within-host evolution of *Pseudomonas aeruginosa* reveals adaptation toward iron acquisition from hemoglobin. *mBio* **5**, e00966-00914
31. Nguyen, A. T., O'Neill, M. J., Watts, A. M., Robson, C. L., Lamont, I. L., Wilks, A., *et al.* (2014) Adaptation of iron homeostasis pathways by a *Pseudomonas aeruginosa* pyoverdine mutant in the cystic fibrosis lung. *J. Bacteriol.* **196**, 2265–2276
32. Little, A. S., Okkotsu, Y., Reinhart, A. A., Damron, F. H., Barbier, M., Barrett, B., *et al.* (2018) *Pseudomonas aeruginosa* AlgR phosphorylation status differentially regulates pyocyanin and pyoverdine production. *mBio* **9**, e02318
33. Kumar, R., Matsumura, H., Lovell, S., Yao, H., Rodriguez, J. C., Battaile, K. P., *et al.* (2014) Replacing the axial ligand tyrosine 75 or its hydrogen bond partner histidine 83 minimally affects hemin acquisition by the hemophore HasAp from *Pseudomonas aeruginosa*. *Biochemistry* **53**, 2112–2125
34. Barker, K. D., Barkovits, K., and Wilks, A. (2012) Metabolic flux of extracellular heme uptake in *Pseudomonas aeruginosa* is driven by the iron-regulated heme oxygenase (HemO). *J. Biol. Chem.* **287**, 18342–18350
35. Hoang, T. T., Karkhoff-Schweizer, R. R., Kutchma, A. J., and Schweizer, H. P. (1998) A broad-host-range Flp-FRT recombination system for site-specific excision of chromosomally-located DNA sequences: application for isolation of unmarked *Pseudomonas aeruginosa* mutants. *Gene* **212**, 77–86
36. Fuhrop, J. H., Smith, K. M., eds. (1975) *Porphyrins and Metalloporphyrins* (pp. 804–807). Elsevier, Amsterdam
37. Holloway, B. W. (1955) Genetic recombination in *Pseudomonas aeruginosa*. *J. Gen. Microbiol.* **13**, 572–581